May 2025

Wind Turbine Team at Virginia Tech
Turbine Design Report
Collegiate Wind Competition 2025
Virginia Tech, Blacksburg, VA

Prototype Development Team

Anthony Concessi | tonyc1228@vt.edu	**Senior Technical Co-Lead**
Alec Crispino | aleccrispino@vt.edu	**Senior Technical Co-Lead**
Josh Grubb | joshgrubb26@vt.edu	**Power Systems Co-Lead**
Juan Martinez-Medina | juanm04@vt.edu	**Power Systems Co-Lead**
Charlie Elliott | charliegelliott@vt.edu	**Controls Co-Lead**
Tolu Kolade | toluk@vt.edu	**Controls Co-Lead**
Matthew Lewis | mlewis3113@vt.edu	**Mechanical Lead**
Quinn McIver | qmc@vt.edu	**Aerodynamics Lead**

Power Systems & Controls

Leo Bui, Sammy Craypoff, Tom Daggett, Timothy Estrada, Nathan Farmer, Vivian Hazelrigg, Daniel Kang, Walter Lin, Scott Miloy, Reve Meili, JD Putt, Lucas Renfrew, Makeda Solomon, Al Taber, Jordan Talbert, Puneeth Vangamulla, Henry Warfield

Aerodynamics

Arend Austria, Ben Daniel, Louis Harris IV, Charles Hughes, Jackson Mosley, Cristene Sellers

Mechanical

Dane Barnes, Chloe DeKorsey, Kate Douglas, Ben Dye, Jozhel Salazar-Espiridion, Scout Tuttle

Float

Javanni Asis, Ankita Gupta

Faculty Advisors

Dr. Nanyaporn Intaratep | nintarat@vt.edu — **Research Assistant Professor**, Kevin T. Crofton Department of Aerospace and Ocean Engineering

Dr. Tim Thacker | tthacker@vt.edu — **Research Associate Professor**, Bradley Department of Electrical & Computer Engineering

ENGINEERING VIRGINIA TECH.

Advanced Engineering Design Lab

VIRGINIA TECH.

Table of Contents

I. Executive Summary & Distributed Team Environment

The Wind Turbine Team at Virginia Tech's goal was to design a small-scale wind turbine that could efficiently generate power while promoting wind energy to the next generation of creative minds. This year, the team's design objectives were to optimize the design of mechanical sub-systems, research and manufacture optimal turbine blades, and create a reliable electrical system while improving upon the efficiency of last year's design. By completing the above objectives, the team has become prepared to successfully perform all Tasks of the 2025 Collegiate Wind Competition (CWC). The team divided work between three subteams to achieve its goals: Power Systems and Controls (PSC), Mechanical, and Aerodynamics.

This year, the PSC subteam was divided into two teams, the Power Systems team and the Controls team, with two leads being appointed to each. Through this year's development, the Power Systems subteam improved upon the efficiency of its variable load. Improving from last year's implementation using MOSFETs as switches, the variable load utilizes relays to maintain the maximum power point of the turbine throughout the entire wind range. The Controls team developed an improved finite state machine (FSM) that enabled variable load control, ensuring the turbine would be as efficient as possible at all competition speeds. Finally, the Power Systems team selected an optimal brushless DC motor as the generator for this year due to its improved efficiency and wide motor selection.

The Mechanical subteam was also split into two groups this year. The Mechanical team focused on optimizing nacelle components to minimize weight and improve the reliability of structure to driveshaft connections, while the float team focused on implementing a stable floating foundation. To meet these goals, the subteam modified the layout of the turbine nacelle structures and iterated a variety of foundation prototypes.

The Aerodynamics subteam researched, designed, optimized, and manufactured the yaw and blades for the turbine. It split its members between blades and yaw/nacelle, focusing on optimizing the blades for turbine side electronics by manipulating the designed tip-speed ratio and reducing the impact of the float on turbine performance.

This report will discuss design improvements, justifications for designs, setbacks, and results from testing the prototype in the Virginia Tech Open Jet Wind Tunnel. It will give an overview of the entire system in parts, then detail how those parts come together to complete the turbine.

II. Turbine Design

A. Pitch Control and Blade Hub

The purpose of the pitch control system is to quickly and reliably adjust the pitch of the blades to optimize the power output of the turbine and ensure that the rotor can stop in the case of an emergency. Taking inspiration from helicopter rotors, our system pitches the blades with linkage bars connected to a swashplate that travels up and down the drive shaft. This is the same method of pitching the blades as last year's design. We chose to keep the design because of its efficient use of space and ease of control.

Shown in Figure 1, this year's new linear actuator is used in conjunction with the previously described swashplate. The team chose this model due to its small step size of 1 mm, which is equivalent to 4.56° per step, allowing for more precise adjustments when controlling pitch angle. A deep groove ball bearing is mounted to the linkage plate and carried by the swashplate assembly. The curved linkages allow for 105° of actuation.

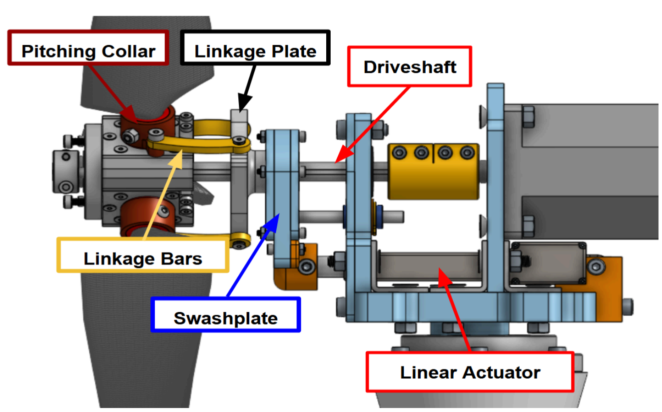

Figure 1: Annotated pitch actuation system

The blade hub shown in Figure 2 is mostly the same design that was used in last year's competition. With the addition of lock-out stoppers, this iteration of last year's design addresses an issue seen from testing. We decided to use this design in this year's competition due to the longer allowable blade length and minimal footprint.

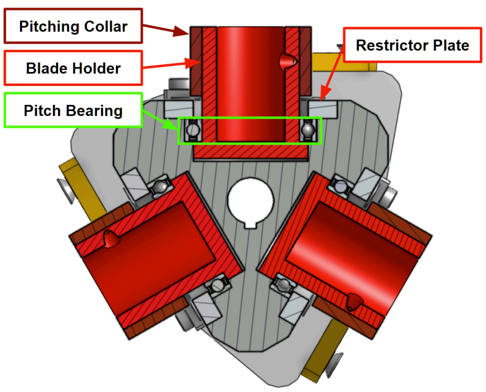

Figure 2: Annotated blade hub assembly.

Last year's hub consistently experienced a lock-out issue. Shown in Figure 3, lock-out would occur when the force acting on the blades overcame the resistant force of the linear actuator. This rotated the pitching collars past the allowable power angle. After this point, it was not possible to pitch the blades. To solve this issue, the team modified the hub design to include mechanical lock-out stoppers that obstruct the backward motion of the linkages. By 3D printing these stoppers, the allowable pitch of the blades can be fine-tuned. Implementing this change has entirely eliminated the possibility of lock-out in our system.

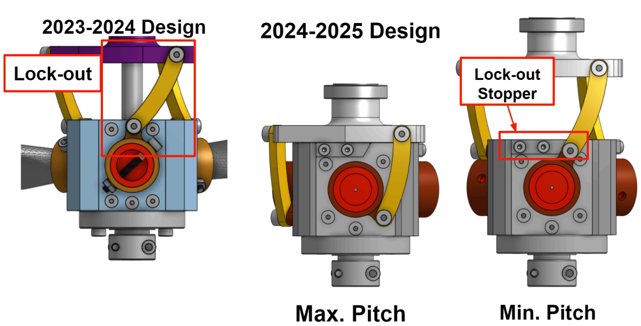

Figure 3: Max. and min. pitched linkages on the hub and engagement of the lock-out stopper.

B. Turbine Nacelle Structures

The structures of the turbine are made of varying thicknesses of 6061 aluminum plating. The plates are fastened to the baseplate with stainless steel corner brackets and a custom front bracket. Expanding upon last year's design, this structural methodology has proven to be versatile and has allowed us to rapidly test different turbine configurations.

To reduce the turbulence of the passing air and to reduce drag leading to complications with the float, the nacelle and nose cone design aimed to employ a holistic approach. This year's iteration completely encloses all non-aerodynamic parts of the turbine, most notably the pitch actuation system, to allow for minimal flow interruptions.

Figure 4 shows configurations for three different generators. Using this plate design, we were able to quickly manufacture plates to mount different components. An equivalent radial load on the forward plate bearing was calculated based on the maximum possible torque at a wind speed of 18 m/s. Using this and the static bending load of the hub when parked, both yield factors of safety were calculated to be >100. Despite being overbuilt, this ensures that our nacelle will be structurally sound throughout testing.

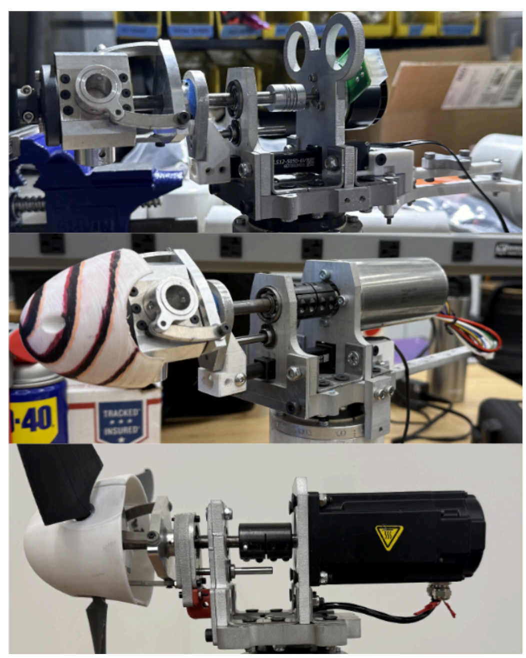

Figure 4: Chronological plate configurations.

Two deep groove ball bearings are mounted to the drive shaft. Shown in Figure 5, the swashplate bearing is mounted onto the linkage plate and is carried by the assembly shown. As the hub rotates and when the blades are being pitched, there is combined loading on the swashplate that needs to be resisted at the swashplate bearing carrier. A bearing carrier was designed to encase the outer race of the deep groove ball bearing. A 0.25-in aluminum plate is flanked on either side by 0.125-in aluminum plates designed to press against the face of the bearing's outer race. The forward plate bearing shown in Figure 5 is under an alternating bending load when the turbine is running. In last year's design, a bearing in the same location was pressure-fitted into the plate. This resulted in the constriction of the bearing's outer race, drastically decreasing the efficiency of the bearing, and causing it to frequently slip out of the mount. A plate was added onto the front of the bearing to come into contact with the front face of the outer race and resist the alternating bending load.

With an offshore foundation implemented in this year's competition, we identified the key priority of minimizing the overall mass of the turbine. This would reduce the moment arm created by the turbine on the foundation, thereby improving stability.

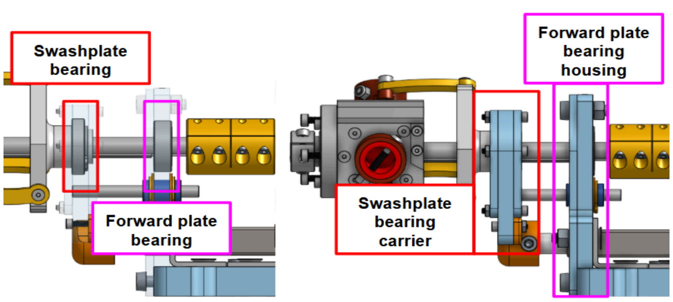

Figure 5: Deep groove ball bearing locations and mounts

To reduce the mass of the turbine, we looked at two of the heaviest parts of the turbine structure. The base plate and the yaw bearing mount were determined to be the biggest single contributors to the overall mass of the turbine. The baseplate is a waterjetted plate of 0.50-in 6061 aluminum. Figure 6 shows the baseplate before and after the milling process and the newly designed yaw bearing mount. Waterjetting made this milling process easy and effective, reducing the mass of the baseplate by 28%. Also machined out of 6061 aluminum, the yaw bearing mount was similarly redesigned. Applying best practices, the yaw bearing's mass was reduced by 43%.

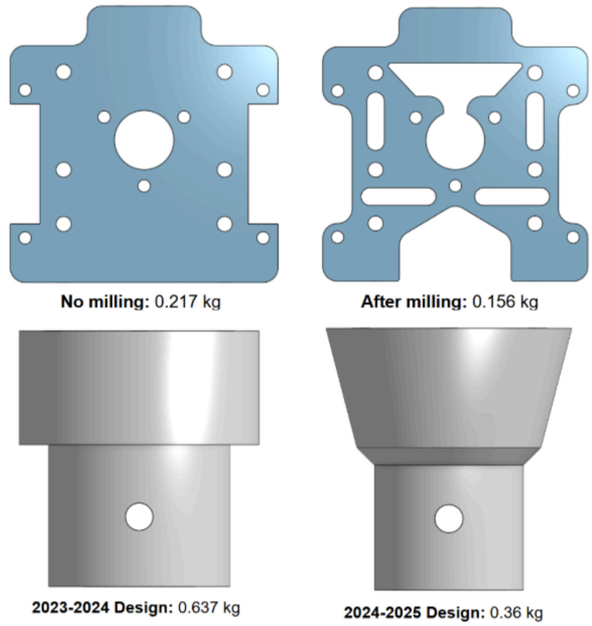

Figure 6: Structures before and after weight optimizations

C. Floating Foundation

1. Design Iterations

Being the focal point of this year's competition, the team spent the majority of the project duration designing and iterating foundation prototypes. These floating foundations were intended to maximize the stability of the dynamic system in the offshore environment while adhering to the specific competition requirements.

At first, the team decided to try to produce two prototypes that mimic well-documented foundation types in the offshore wind industry. These first prototypes used commonly available materials such as schedule 40 PVC piping and sand ballasts. The PVC Spar Buoy and Semi-submersible, seen in Figure 7 (first 2 from left), were designed to have the most displacement using individual pipes, staying within the physical limits of the competition. These initial prototypes were not able to stabilize in the water under unloaded conditions and experienced additional challenges, such as leakage and difficulty when installing mooring lines.

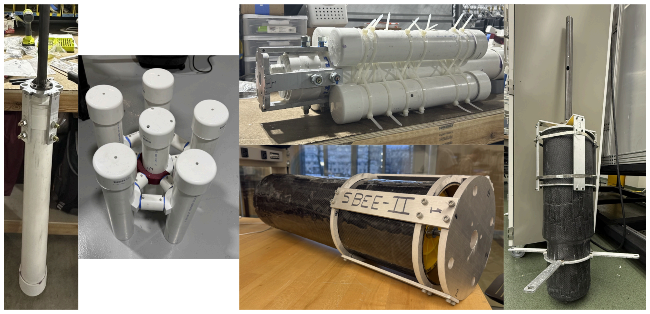

Figure 7: Floating foundation designs: PVC Spar Buoy (left), PVC Semi-submersible, SBEE-I (upper middle), SBEE-II (lower middle), and SBEE-III (right).

The next iteration of our offshore foundation analyzed the centers of buoyancy (CB) and gravity (CG). Combining the material from the previous PVC foundations, the Spar Buoy Extended Edition Mk.1 (SBEE-I) seen in Figure 7, was designed around this criteria. The CB was raised by displacing more volume at the top of the buoy and closer to the waterline (the desired center of rotation). Figure 8 shows the distance between the CB and CG as a function of addDed PVC cells. As the displacement at the top of the buoy is increased, the difference increases, validating the design philosophy.

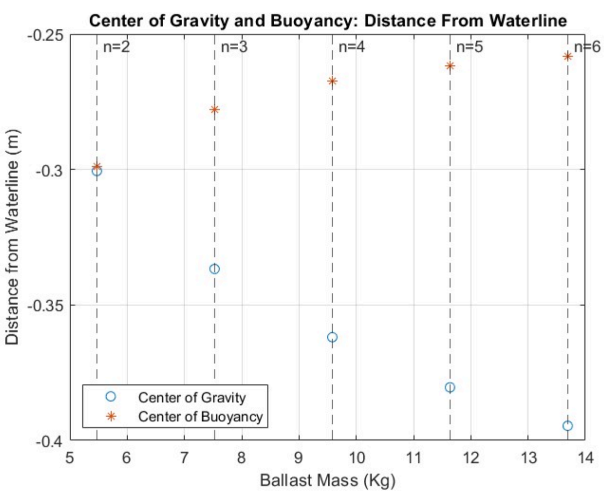

Figure 8: Variation of the Spar Buoy Extended Edition Mk.1 (SBEE-I) centers of gravity and buoyancy with the addition of exterior PVC cells.

Testing the SBEE-I continued to validate the design, however, it failed to sustain the mass of the turbine. It was theorized that the comparably large distributed mass of the PVC was severely limiting the manipulation of the CG. Table 1 shows the material properties of two composites considered for the body, as well as PVC. Because of how thick the PVC piping was, only comparing the density of the materials would be misleading, as composites are much stronger and allow for thinner walls. Taking the average wall thickness into account and comparing the mass per tube area, we were able to determine that a carbon fiber epoxy composite would be the best choice for the SBEE-II because it minimizes the mass of the body, allowing for greater control of the CG.

Material	**Density (g/cm^3)**	**Average Wall Thickness (cm)**	**Mass/Tube Area (g/cm^2)**
PVC	1.4	0.7	0.98
Carbon Fiber Composite	1.15 - 2.25	0.18	0.207 - 0.405
Fiberglass Composite	2.54-2.6	0.42	1.07 - 1.09

Table 1: Properties of considered materials [2].

For SBEE-II and SBEE-III, the team revisited the foundation stability calculations and modified them to calculate the metacentric height, which provides a better grasp of resistance to heeling compared to analyzing the center of gravity and buoyancy. Matlab was implemented to iterate several designs before manufacturing them. The mooring lines were not factored into the calculations due to the complexity introduced when estimating the dynamic response, although the amount of excess buoyancy necessary to maintain the desired mooring line tension (no more than half the weight of each mooring weight) was found and applied to the total volume of the spar.

For SBEE-II, the team decided on a foundation length of 75 cm based on the competition tank water depth of 83 cm ± 1 cm to achieve a high buoyancy force while maintaining a margin of error for collision with the tank floor and mooring weights. The diameter of the foundation was chosen to be 20.32 cm (8 in) as it would allow us to keep the center of gravity low without requiring an unmanageable amount of ballast weight. When the SBEE-II was constructed, imprecise manufacturing techniques led to it being approximately 3 cm longer than intended, partially causing it to bottom out during testing, along with unaccounted weight from the tower mounting apparatus. The calculated ballast weight was determined using the MATLAB script such that the waterline of the buoy was equal to the total height of the buoy.

The stability of a vessel can be modeled by calculating the metacentric height (GM), also known as the distance between the metacentre and the center of gravity. The metacentre is the point at which the resultant line of buoyancy force, once the system is tilted, intersects with the original line of buoyancy force (an axial line through the buoy). The larger the distance GM is, the more stable the vessel should be. GM can be calculated using the equation:

$$GM = KB + BM - KG$$

where KB is the center of buoyancy in relation to the bottom of the foundation, BM is the metacentric radius, and KG is the center of gravity in relation to the bottom of the foundation.

For SBEE-III, the team altered SBEE-II, making two-thirds of the upper section of the foundation a 25.4 cm (10 in) diameter tube that tapers down to a 20.32 cm (8 in) tube to increase the buoyancy force and raise the center of buoyancy. Table 2 shows stability calculations of the GM with different buoy body proportions. One criterion guiding this process was the goal to repurpose a portion of the 20.32 cm (8 in) SBEE-II in order to conserve limited materials. With this design, the ballast weight was reduced to 17 kgs to allow the mooring weight configuration enough excess buoyancy to keep the mooring lines in tension.

Portion of 8-in. Tube Used	Calculated GM
100%	1.6432
66.6%	1.7277
50%	1.7654
33.3%	1.8006
0%	1.8647

Table 2: Stability of SBEE-III based on the portion of SBEE-II used.

The team also reconsidered the orientation of the mooring lines with respect to turbine stability. To approach this, we researched the use of Tension-leg Platforms/Buoys, which use excess buoyancy to maintain tension in a set of mooring lines, thereby impeding vertical motion and greatly enhancing overall stability [1]. The process resulted in four 9-in-long 6061 aluminum mounting spokes being designed to extend outward from below the transition point on the spar. Each arm is fastened to a segmented 6061 aluminum mounting ring using screws. The mounting location was chosen as an effective intermediary between creating the largest possible restoring moment and serving as an easily accessible point during installation. Testing revealed that placing the mooring lines at an incline led to the lowest results for horizontal deflection and tilt angle, and eliminated the instability that previous float designs demonstrated at equilibrium.

2. Specialized Tools

To efficiently install the floating foundation, we created a set of tools that limited the margin of error and risk of failure modes.

To interact with the mooring weight rigs without touching the water, the team manufactured variable-length pole hooks using telescopic poles and plastic boat hooks. Figure 9 shows these manufactured installation tools. Plastic chain was chosen as a mooring line material due to its acceptable axial stiffness and ease of measurement. Loops of paracord were used to create a spring-loaded mechanism for each of the carabiners. These loops are lifted up with the pole hook, locking the carabiner.

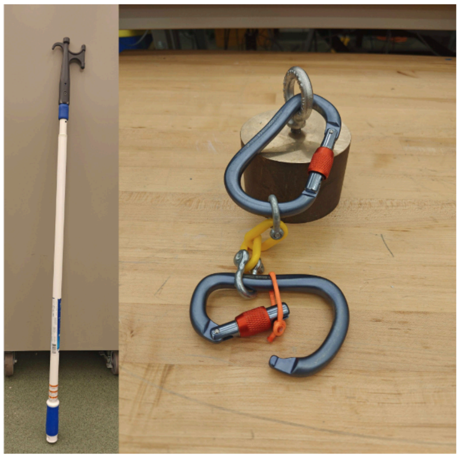

Figure 9: Pole hooks (left) and spring-loaded carabiners/mooring chains (right)

D. Blade Design

To determine design parameters for blades, the wind speed was calculated with the competition's scoring weights to select the design wind speed to be 8 m/s. The optimum tip speed ratio (TSR) was used to get the minimum required RPM at the competition's lowest wind speed to produce a minimum voltage of 10V to power turbine side electronics. For the Kollenmorgan generator, the minimum TSR was found to be 4.1; however, the team decided to reduce the design TSR to 3 to compensate for the TSR's effect on cut-in, and to still achieve peak performance at 8 m/s.

To select the appropriate airfoil geometry, the team considered peak lift to drag ratio, structural performance, and cut-in speed. This year, we tested several dual airfoil configurations for blade shape, with the SG6043 at the root half of the blade, and varying other airfoils at the tip half of the blade. The SG6043 was chosen for its structural properties and its excellent aerodynamic characteristics. This hybrid configuration was chosen to theoretically combine the performance of the SG6043 at low wind speeds with a higher Reynolds Number airfoil for the higher wind speeds. Further, the improved structural rigidity helps with 3D printing performance, resulting in better printing of blade geometry, notably a thinner trailing edge.

To compare with blades made with a purely SG6043 blade, we generated 14 distinct blades in QBlade software, utilizing the A18, BW-3, S1223, SD7003, E387, and E64 airfoils chosen from Singh's research on low Reynolds Number airfoils [3], and optimizing their chord length and twist with QBlade's Schmitt optimization. Using QBlade's built-in simulation software, each blade was tested at our predetermined optimum wind speed. Of the tip airfoils selected, the Eppler 64 (E64) showed the most promise, having a lower cut in speed and better peak power than other blades.

Using wind tunnel testing to verify the simulation, the hybrid E64/SG6043 did achieve the highest peak power of 31.5 watts at 11 m/s**;** however, due to its performance compromises at lower wind speeds, the purely SG6043 blades at the same TSR scored nearly 3 points higher. Therefore, the team chose a purely SG6043 as the blade geometry to further iterate.

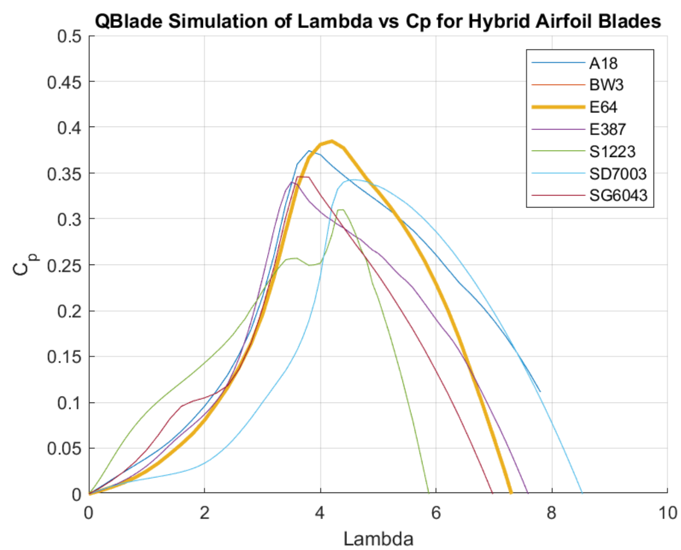

Figure 10: Hybrid Blade QBlade Simulations

To further improve the performance of the blades, the SG6043 blade was modified to include a winglet with a 45-degree cant angle that was determined by Zhang to be the optimum [4]. Sweeping the winglet upward and twisting the blade can enhance aerodynamic efficiency by reducing tip vortex strength, which is a major source of energy loss. This design helps minimize induced drag and improves the overall power output of the turbine, especially at lower wind speeds. After testing a modified

SG6043 blade with a TSR of 3, the peak power output increased by nearly 10%, corresponding to a one-point total increase. This reduction in tip vortices also increased the stability of the yaw in experimental testing. As shown in Figure 10, nearly every wind speed tested showed an increase in power output. Shown in Figure 12 are the geometry changes made to the blade.

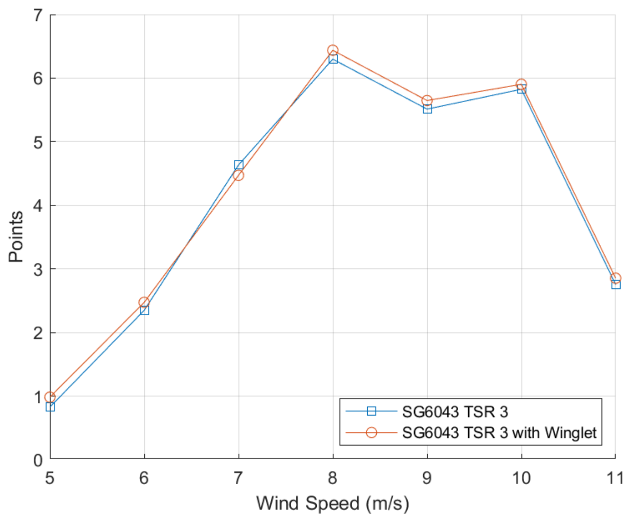

Figure 11: Competition points from QBlade default and modified winglet blade design vs. wind speed

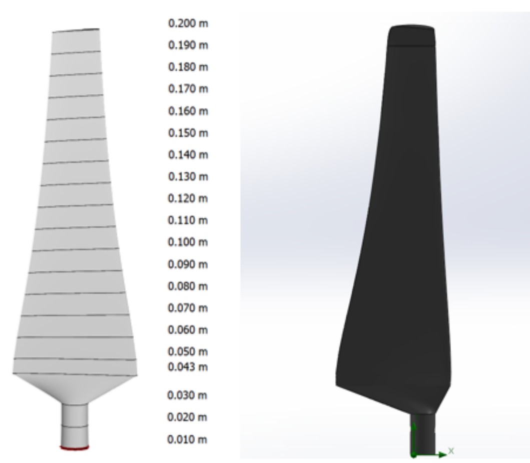

Figure 12: QBlade default vs. Modified Blade with Winglet

To fabricate each blade, the team used PLA-CF, chosen for its added rigidity over ordinary PLA with a bending modulus of 3380 MPa vs. 2894 MPa, respectively [5, 6]. PLA-CF also showed significant performance benefits shown in Figure 13, over last year's chosen filament, CF-infused ONYX plastic, likely due to its significantly improved surface roughness. Therefore, PLA-CF was used to fabricate the final blades.

Using the average wind speed found for the offshore location chosen in the project development report, 10.875 m/s at 120 m above sea level, this turbine would generate an estimated 112.5 kWh per year.

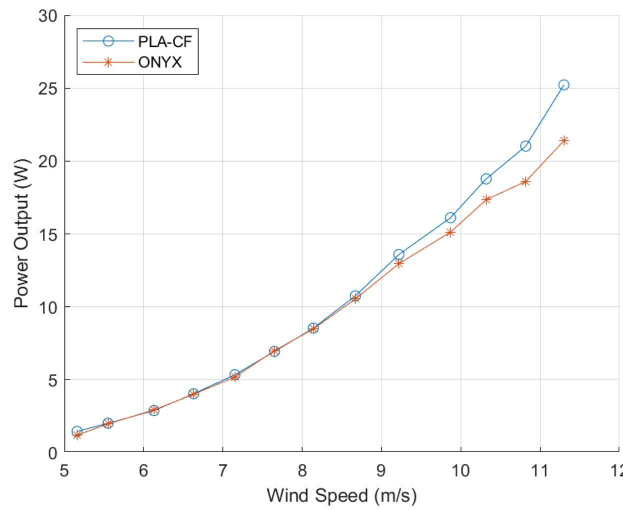

Figure 13: Last Year's ONYX Blades compared to the SG6043 TSR 3 PLA-CF blade used as a basis for the winglet design

E. Yaw Design

To compensate for the dynamics of the float, a swept PLA NACA 0008 double-vane yaw configuration with an inward angle of attack offset of 10 degrees was selected due to its symmetrical profile and dependable aerodynamic performance, ensuring stability and predictable response across all competition wind speeds. Several other two yaw vane configurations were tested including, a NACA 0012 airfoil with a wingspan of 200 mm and aspect ratio of 3.6, then two NACA 0008 vane designs, each with a wingspan of 281.25 mm and a variable aspect ratio of 5.4 and 9.4. All initial designs exhibited substantial aeroelastic issues in the wind tunnel, notably fluttering at higher wind velocities, which reduced the effectiveness of the yaw control.

To address these aeroelastic challenges, the final vane design integrated the chord dimensions from the NACA 0012 vane and the larger wingspan from the NACA 0008 variant, included internal structural reinforcements, and optimized the placement of the yaw through CFD analysis. Specifically, internal ribs and spars were added to enhance stiffness and reduce flutter. This structural improvement allowed the system to fully utilize generated lift, resulting in improved yaw stability and reliable centering of the turbine at lower wind speeds. Using CFD allowed us to find the optimal distance from the center to place our yaw vanes. This distance came out to be 75 mm from the center on both sides to maximize our relative velocity while reducing the amount of tip vortices the vane experienced.

To further optimize the yaw for the float, the team focused on keeping designs as light as possible, integrating all support for the yaw into the nacelle design. As shown in Figure 14, the nacelle extends to provide mounting support, reducing the need for heavy, metal components.

Another major design feature of the yaw is its utilization of drag as a contributor to the moment. Using a vortex lattice theory, the yaw moment per vane was calculated to be 1.05 Nm with zero nacelle deflection at 5m/s without including rotor effects, with a generated force of 6 N and 0.3 of drag.

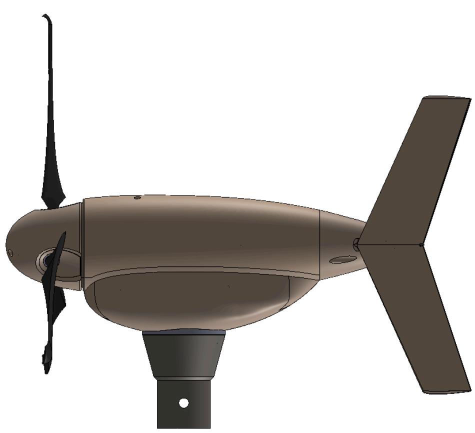

Figure 14: Double Vane NACA 0008 Yaw Design on Final Turbine Assembly

F. Generator Selection

Throughout the design process, multiple motors were tested for the system. Using data from last year, a typical rotor rpm at every wind speed was found. Noting differences in motor specifications and blade design, this data was used to inform generator selection. After extensive research, two main motor options were chosen to be compared through further testing: the Maxon EC-i 52 and the Kollmorgen AKM22G, both brushless motors.

The Maxon EC-i 52 is rated for 200 W at a nominal voltage of 48 V, weighing in at 1.15 kg. This motor has a torque constant of 115 mNm/A and a speed constant of 83.3 rpm/V, leading to a speed/torque gradient of 0.172 rpm/mNm. The Kollmorgen AKM22G is rated for 220 W at a nominal voltage of 75 V, weighing in at 1.1 kg. This motor has a torque constant of 180 mNm/A and an estimated speed constant of about 35 rpm/V at 75 V, leading to an estimated torque gradient of 0.688 rpm/mNm. These values were estimated using rated rpm at a given voltage and the torque versus speed plot provided in the Kollmorgen AKM22G datasheet.

The EC-i 52's lower torque constant and higher speed constant suggest that it would perform with better efficiency at lower wind speeds, but taper off in performance at the higher speeds. The AKM22G's characteristics suggest the opposite, although its higher torque gradient suggests it will experience a slower drop in speed as the motor's mechanical load is decreased (electrical load seen by the motor is increased). This could mean that the motor performs better across the entire wind range, especially at higher wind speeds.

The blade airfoil used last year was determined to be a suitable middle ground between speed and torque characteristics and was used atop a static test bed configuration to establish identical testing conditions for both motors. A constant load was connected across the rectified generator output, and a computer was connected directly to the turbine-side Arduino, enabling complete manual control over the turbine. Complete power curves were conducted for numerous loads to find the optimal load for each wind speed.

WS (m/s)	CWC Points (EC-i 52)	CWC Points (AKM22G)
5.16	0.55447	1.042972
6.13	1.7627328	2.646345143
7.15	3.4857216	5.0176
8.14	5.0433656	6.56915
9.22	4.66480624	6.0552
10.32	5.096680104	6.562323
11.3	2.366451235	2.927521
Total:	**22.97422758**	**30.82111114**

Table 3: CWC points for each generator for maximum power seen near competition speeds

Table 3 shows that the AKM22G was able to produce a higher competition score, while Figure 15 displays each generator's power curve overlaid on each other.

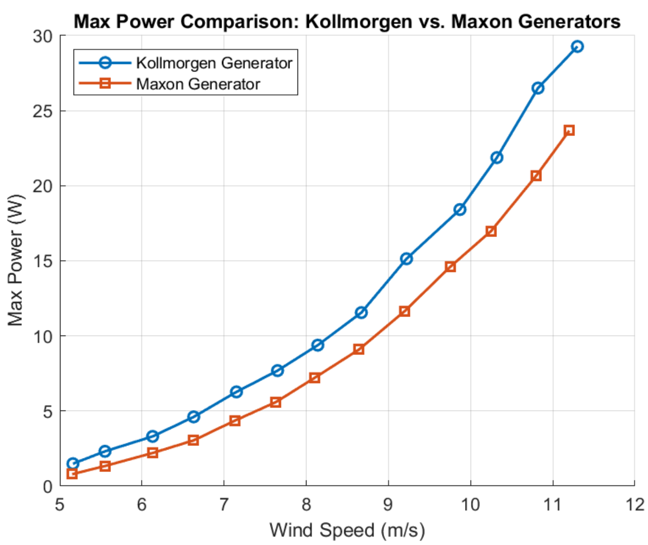

Figure 15: Maximum power curves for each generator from testing data

Although the characteristics of the EC-i 52 motor may have implied better performance at lower wind speeds, the AKM22G's better performance across the wind range could be attributed to inaccuracies in its datasheet, as it is a retired model. Based on the evidence presented above, the Kollmorgen AKM22G was selected to be the generator utilized in the final implementation.

G. Electrical Systems

1. Turbine Side

Figure 16 below shows the turbine side electronics, which ensure that the generator's output can be used and measured at the PCC. An off-the-shelf diode bridge rectifier converts the brushless DC motor's three-phase output to DC, which is then smoothed by a bulk capacitance. A relay is connected to the positive DC bus (PCC+) such that its normally open (NO) and normally closed (NC) pins connect to an Arduino UNO R4's Vin pin and an off-the-shelf buck converter's positive input, respectively. The buck converter's negative input connects to the negative DC bus (PCC-), with its output set to 9 V and serving as a voltage input for the Arduino and the safety relay coils. Relays switched by Arduino digital pins connect directly to the generator's three-phase output with their NO pins connected through low-valued power dissipation resistors to PCC- for the safety task. The Arduino's 5 V pin powers a boost converter set at 6 V, which feeds the linear actuator. A voltage divider connects across the PCC to inform the Arduino of the system's bus voltage, and a CubeCell LoRa module communicates with the load-side Arduino.

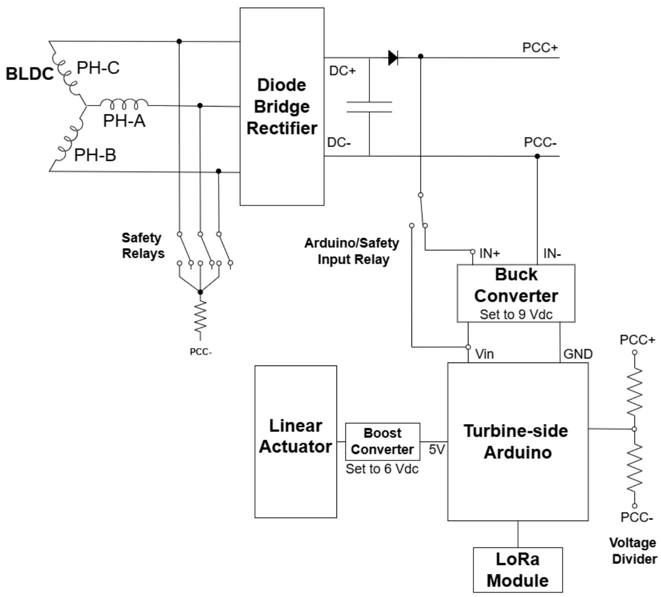

Figure 16: Turbine-side electronics one-line

During the turbine's cut-in period, the system receives 12 V from the load side's wall-fed 12 V supply through the PCC, keeping the Arduino on while the turbine ramps up in speed. To prevent backfeed into the rectifier, a diode is placed between PCC+ and the buck converter input. The Arduino input relay is switched on during this state, powering the buck converter to step down the 12 V to 9 V to coincide with the safety relays' coil ratings. After transitioning into POWER state, the backfeed and Arduino input relays are switched off, powering the Arduino and safety relays with PCC+ until it surpasses 10 V. The Arduino input relay is then switched back on to step down its input voltage again, ensuring that it and the safety relays only receive voltages in their input range.

The linear actuator is controlled via the Arduino and its native servo library. The library allows the Arduino to emit a PWM signal with a certain pulse width for the linear actuator (925–1925 µs). The actuator is initialized to its home position at startup by sending a 925 µs pulse. Through testing, we found that incrementing the PWM pulse width by 25 µs corresponds to a 1 mm actuation.

2. Load Side

Figure 17 below shows the load side electronics, which provide a dynamic resistive load to the turbine to optimize its power output. A 50Ω load sits across the PCC to serve as our starting load and ensure that the turbine never enters a runaway state. In parallel are several relays supplied by the 12 V supply that can be powered on individually and add load, reducing the resistance seen by the turbine side as the wind speed increases during the Power Curve Performance Task. Optimal loads for each wind speed are pre-determined through extensive testing, with the relays switched by a load-side Arduino UNO R4 that obtains a voltage reading with a voltage divider connected across the PCC.

A relay placed between PCC+ and the positive 12 V supply output allows for control of a backfeed system. When switched on, it sends 12 V through the PCC and to the turbine side to keep its electronics powered during the cut-in period or an E-STOP-activated safety mode.

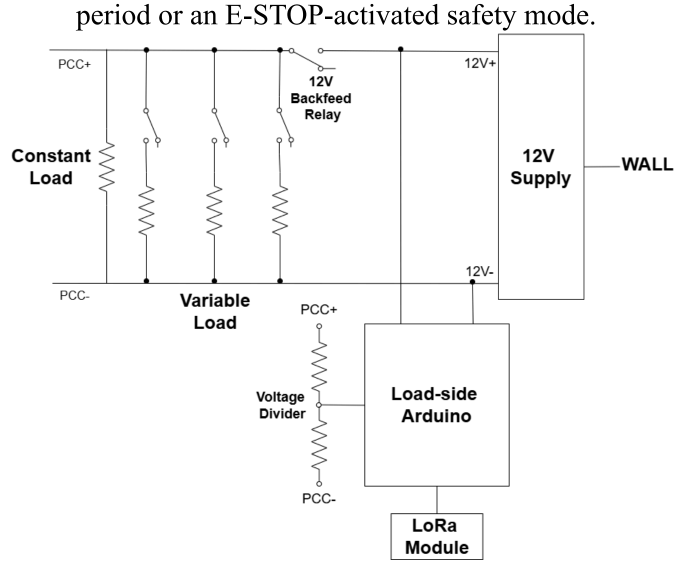

Figure 17: Load-side electronics one-line

3. Inter-Enclosure Communications

Two-way communication prototypes utilizing WiFi and LoRa were made to select the most optimal model for the turbine to establish a communications link between the turbine and load side enclosures. With WiFi, one Arduino serves as a host and the other as a client with their built-in ESP32-S3 chips, such that packets can be sent between the two Arduinos. LoRa, standing for 'Long Range', utilizes an external module to enable UART communication between Arduinos.

After extensive testing that included distance, transmission speed, error, and loss rates analysis, LoRa was ultimately chosen as the best for the turbine for several reasons. These include its exceptional range and signal penetration, resistance to ambient noise and interference, low power consumption, and readily available Arduino libraries. This implementation allows for either Arduino to transmit data to the other or trigger an FSM state change. Before integrating the modules with the turbine system, their capabilities were demonstrated by reliably communicating the resistances of a series of potentiometers through LoRa to power certain components of an LED array.

On the turbine side, the LoRa module is responsible for transmitting important operational data, including voltage at the PCC and the FSM state. This information is sent at regular intervals or is triggered by specific conditional events, ensuring that the load side is always up to date with turbine conditions.

On the load side, the LoRa module receives relevant turbine information and, based on the information received, makes a real-time decision about load switching and protection measures, then sends information or status updates back as needed. A compact LED display is used to monitor the status of the load side, where a numerical range informs us which variable load relays are active, and color-coded indicators monitor the FSM state of the load side, quickly informing the user of any potential issues within the system.

III. Software

A. Finite State Machine

Two separate finite state machines (FSMs), one on the turbine side and another on the load side, were implemented for the system. Both utilize similar control structures but operate based on different input conditions and control operations. Each FSM cycles between 3 states: CUT_IN, POWER, and SAFETY, as seen in Figure 18. Figure 19 displays the system UML diagram and goes into further detail about the interaction between load and turbine sides, including pitch and display control.

The system starts in a CUT_IN state and enters a low-activity mode. Load-side electronics keep all variable load relays switched off, minimizing generator load, while the 12V backfeed relay is switched on to provide power to the turbine-side electronics. The turbine side Arduino input relay is switched on, powering the linear actuator to pitch to an optimal cut-in angle. Meanwhile, the turbine monitors the PCC bus voltage on both sides, waiting for it to exceed a voltage threshold before incrementally decreasing the blade pitch angle and entering POWER. In the case of a time-out in LoRa communications, an E-STOP press, or a load disconnect, the system enters SAFETY.

Entering the POWER state, the 12V backfeed relay and Arduino input relay are switched off, and the bus voltage at the PCC on the load side is monitored to inform variable load relay switching. Once the PCC bus voltage on the turbine side exceeds 10V, the Arduino input relay is switched on. The turbine side Arduino monitors the voltage at the PCC to inform pitch angle changes, as needed. In the case of a time-out in inter-enclosure LoRa communications, an E-STOP press, or a load disconnect, the system enters SAFETY.

In an E-STOP-activated SAFETY state, the turbine side Arduino immediately pitches the blades to produce a negative torque, the safety relays are switched on to short the generator phases together, the 12V backfeed relay is activated to keep the turbine side electronics active, and all variable load relays are activated to increase generator load. In a load disconnect-activated SAFETY state, the Arduino will only pitch the blades to avoid sudden torque spikes in the generator caused by quickly switching the safety relays back off when it loses its power source. If E-STOP is unpressed or the load is reconnected, the system enters CUT_IN.

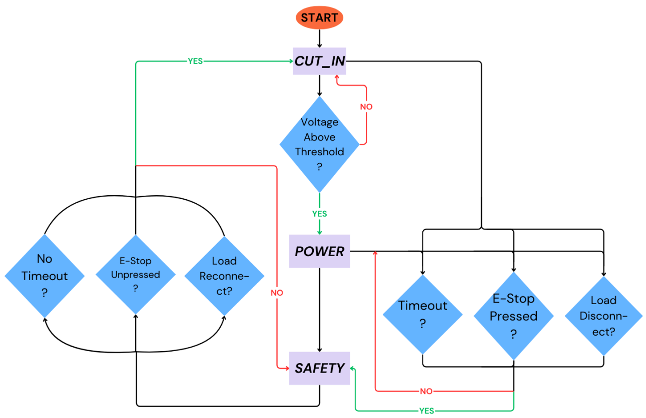

Figure 18: Finite state machine flowchart

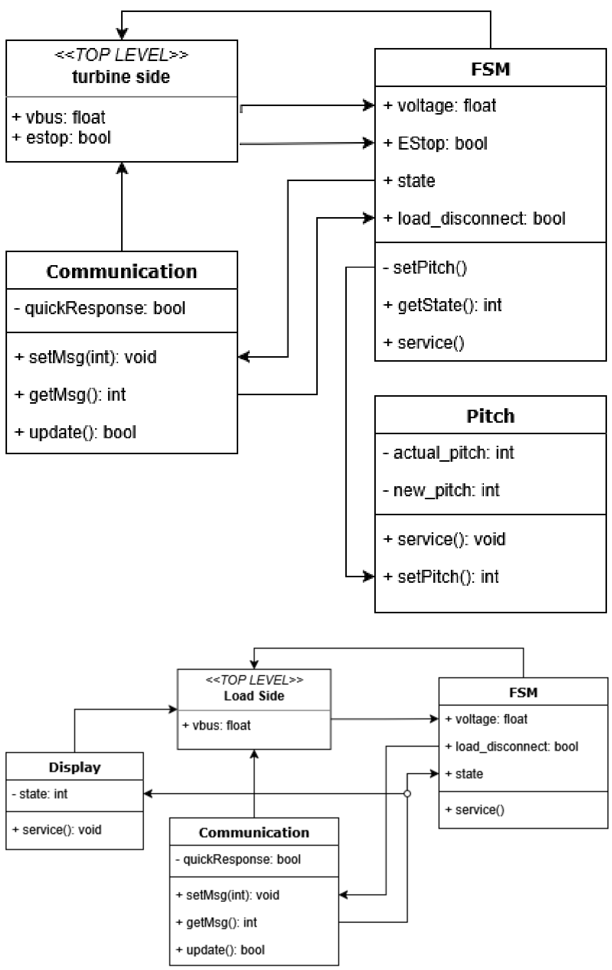

Figure 19: System UML diagram

B. Safety State Activation Detection

To detect an E-STOP press, either end of the E-STOP connector interfaces with a turbine-side Arduino digital pin, and a continuity check is performed. If an open circuit is detected, the E-STOP is assumed to have been pressed, and the system enters SAFETY.

A load disconnect is detected in POWER when the PCC voltage reading on the load side is approximately 0V, in which case the load-side Arduino will communicate through LoRa to trigger a SAFETY state in the turbine-side Arduino.

V. Complete System Testing

Using the wind tunnel, we were able to successfully conduct a full competition-specification system test, including Power Curve Performance, Safety, and Float and Mooring Success Tasks.

The generated power curve from our Power Curve Performance Task test can be seen in Figure 20. As shown previously in Figure 11, we ultimately scored 28.77 points when using competition weighting, with a peak power of 31.25W. The Safety Task was tested at up to 13 m/s, where the turbine successfully slowed to a near-complete stop in under five seconds. The Float and Mooring Success Task was tested at up to 22 m/s, where the tower deflected approximately 1 degree.

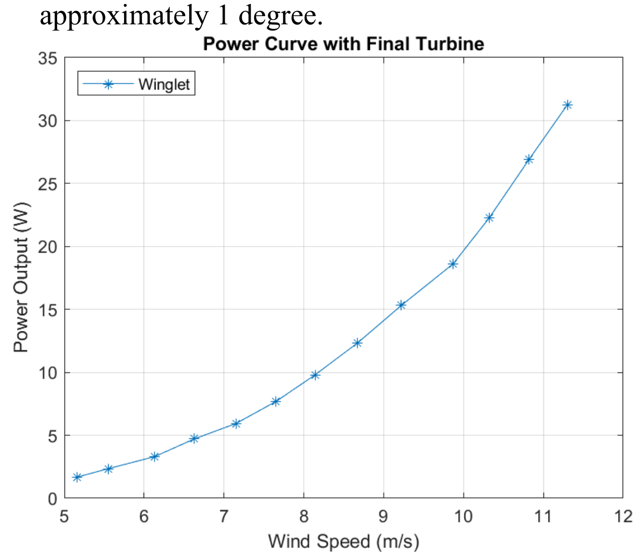

Figure 20: Final Turbine Power Curve

V. Assembly and Commissioning

A. Final Assembly

The full system is divided into three primary components: the nacelle, tower, and floating foundation. The nacelle constitutes the blades, hub, pitch control system, and generator. All individual components are structurally supported by aluminum plating and enclosed by a 3-D printed outer casing. This assembly is fastened to the tower by a mount containing a deep-groove ball bearing to enable yaw capabilities. The tower stub is connected to the floating foundation via three mounting stubs protruding from the top mounting plate. To connect external electronics to the turbine, wiring is fed through the tower, bearing mount, and into the nacelle assembly.

B. Installation/Commissioning Checklist

Before the installation of the floating foundation, we will affirm the following:

- ☐ Nacelle structures, including electrical components, are fully assembled (Generator, Linear Actuator, Hub/Pitch System, Nacelle Shell, Yaw) and fastened to bearing mount
- ☐ Generator cables, linear actuator cables, and their corresponding connectors are in good condition
- ☐ SBEE-III contains all required ballast weights, is sealed by an inside-of-pipe gripper plug, and aluminum mounting components are secured
- ☐ Blades are in good condition and all sit at the same angle
- ☐ Spring-loaded carabiners are attached to mooring lines and preset in an unlocked position

Once these preliminary conditions are met, the team can proceed with formal Installation Tasks. Each task will be confirmed and simultaneously verified by two team members.

Installation Task	**Team Member #1**	**Team Member #2**
Raise floating foundation through tunnel door and into water tank without contacting waterline		
Using pole hooks, carry mooring weight rigs into water tank and attach to mounting spokes		
Adjust mooring lines and ensure carabiners are in the locked position		
Feed electrical connections through tower and mate generator and linear actuator cables		
Fasten bearing mount to tower without disrupting internal connections		
Move tower and nacelle into water tank		
Secure tower to floating foundation		
Make final adjustments such that the buoy center is laterally biased in the front half of the watch circle		
Adjust nosecone to face wind direction		
Mate turbine and load side PCC cables at PCC		
Connect E-STOP connector to mating connector at PCC		

Connect 12V supply wall power cable		
Verify status lights on both Arduinos and LoRa modules		
Ramp wind speed to 5 m/s. Verify accurate state switch from CUT_IN to POWER, including pitching, 12V backfeed relay operation, and Arduino input relay operation		
Disconnect load and verify accurate state switch to SAFETY. Ensure that all expected SAFETY functions are completed		
Reconnect load and verify accurate state switch to CUT_IN, then POWER. Ensure that all expected CUT_IN and POWER functions are completed		
Press E-STOP and verify accurate state switch to SAFETY. Ensure that all expected SAFETY functions are completed		
Turn off wind tunnel. After wind has stopped, unpress E-STOP		

References

[1] A. Myhr and T. A. Nygaard, “Experimental results for Tension-Leg-Buoy offshore wind turbine platforms,” journal-article, Nov. 2014. [Online]. Available: https://publications.isope.org/jowe/jowe-01-4/JOWE-01-4-p217-mmr06-Myhr.pdf

[2] T. Beachdog, “Carbon vs. Fiberglass,” *Goodwinds.com*, Jun. 19, 2024. https://goodwinds.com/composite-resources/carbon-vs-fiberglass-2/#:~:text=Carbon%20composites%2C%20depending%20on%20the%20resin%20used,density%20of%20around%201.15g/cm3%20to%202.25%20g/cm3.&text=The%20density%20of%20E%2DGlass%20fiberglass%20is%202.54,still%20lower%20than%20steel%2C%20aluminum%2C%20or%20titanium

[3] “Design of a low Reynolds number airfoil for small horizontal axis wind turbines,” *Science Direct*, Jun. 2012. https://www.sciencedirect.com/science/article/pii/S0960148111005325 (accessed May 01, 2025).

[4] J. Johansen and N. Sorensen, “Aerodynamic investigation of winglets on wind turbine blades using CFD,” *osti.gov*, Feb. 2006. https://www.osti.gov/etdeweb/servlets/purl/20752587#:~:text=The%20height%20of%20the%20winglet,a%20rectangular%20tip%20was%20assumed (accessed May 01, 2025).

[5] Polymaker, “Technical Data Sheet V5.4 PolyLiteTM PLA-CF.” [Online]. Available: https://polymaker.com/wp-content/uploads/lana-downloads/PolyLite_PLA-CF_TDS_EN_V5.4.pdf

[6] Ultimaker, “Ultimaker PLA Technical data sheet,” Apr. 2022. [Online]. Available: https://um-support-files.ultimaker.com/materials/2.85mm/tds/PLA/Ultimaker-PLA-TDS-v5.00.pdf